organoids

MDPI

Article

Organoid Culture Using Single-Layer Matrigel Method Recapitulates Cervical Cancer Subtypes In Vitro—A Tool for Precision Medicine Applications

Surbhi Singla [1], Rashmi Bagga [2], Radhika Srinivasan [3], Prateek Bhatia [4,*] and Shalmoli Bhattacharyya [1,*]

[1] Department of Biophysics, Post Graduate Institute of Medical Education and Research, Chandigarh 160012, India; singlasurbhi97@gmail.com
[2] Department of Obstetrics and Gynecology, Post Graduate Institute of Medical Education and Research, Chandigarh 160012, India; rashmibagga@gmail.com
[3] Department of Cytology and Gynecological Pathology, Post Graduate Institute of Medical Education and Research, Chandigarh 160012, India; drsradhika@gmail.com
[4] Department of Pediatrics, Post Graduate Institute of Medical Education and Research, Chandigarh 160012, India
* Correspondence: prateekbhatia16@gmail.com (P.B.); shalmoli2007@yahoo.co.in (S.B.)

Abstract

Advanced cervical cancer remains a major cause of mortality in women worldwide as it has limited treatment options and recurrence is very common. This highlights the necessity to develop patient-derived organoids (PDOs) as preclinical models that can recapitulate the clinical heterogeneity of the cancer in terms of molecular features and genetic background. The PDOs have potential for guiding personalized treatment in clinical practice. In this study, we have established patient-derived cervical cancer organoids from biopsy samples of five patients with two different histological subtypes (squamous cell carcinoma and adenocarcinoma) using a modified protocol. The organoids were characterized to assess their genetic and phenotypic similarity to the parental tumor tissue. The organoids developed in vitro preserved several characteristics of the parental tumors, including histological features, HPV status and a subset of genomic alterations. The expression of cervical cancer-related genes, including PIK3CA, MET, and LRP1B, was found to be comparable between the organoids and the parental tumor tissue. Moreover, characterization of the PDOs after cryopreservation showed the histopathological features of the parental tumor tissue. This study demonstrates that the CERvical Cancer OrganoidS (CERCOS) established using the current protocol hold potential to serve as a platform for personalized medicine.

Keywords: cervical cancer; patient-derived organoids; in vitro 3D culture; single-layer matrigel method; personalized medicine; preclinical model

Academic Editor: Roberto Benelli

Received: 31 July 2026
Revised: 29 August 2026
Accepted: 10 September 2026
Published: 15 September 2026

1. Introduction

Cervical cancer has been a global threat due to its high recurrence rate. Patients often develop resistance to chemo- and radiotherapy, leading to tumor relapse, while some patients do not respond to these therapies at all. The response of the patients to therapy is quite unpredictable, and by the time treatment failure becomes evident, the patient has already progressed to the advanced stage. Many drugs that show promising results during laboratory studies fail during clinical trials. This shortcoming can be attributed to the fact that many cancer models poorly recapitulate the patient's tumor, which hinders

the translation of scientific knowledge from bench to bedside. In the last few decades, organoid technology has emerged as a powerful tool with broad applications in basic cancer research. Patient-derived organoids (PDOs) are known to replicate the genetic, phenotypic, and functional characteristics of the parental tumor, making a highly relevant model in advancing personalized medicine [1]. As a functional model that can mimic the multi-omic characteristics and drug sensitivity of the original tumor, PDOs can be employed as an in vitro substitute for novel drug development. PDOs have been successfully established and used to predict the chemotherapy or targeted therapy response in various cancers, including breast cancer, pancreatic cancer, lung cancer, rectal cancer and ovarian cancer [2–10]. PDOs provide a platform for customization of cancer treatment for precision/personalized medicine by taking individual heterogeneity into account. This can improve therapeutic efficacy with the least drug side effects and reduce the treatment costs.

In this study, we have developed cervical cancer PDOs as a representative preclinical in vitro model that can retain the molecular and phenotypic landscape of the original cervical tumor. Earlier, Villa et al. had established organoids from isolated human cervical keratinocytes using an organotypic raft culture method [11]. This method involved the establishment of a keratinocyte cell line from patient tissue, followed by the generation of organoids from the cell line. This was a relatively time-consuming method, and the cells tend to lose their genetic heterogeneity during 2D culture. Later, Maru et al. (2019) established organoids from a single patient of clear cell carcinoma using a modified Matrigel Bilayer Organoid Culture (MBOC) protocol [12]. In this method, the organoids were sandwiched between two layers of Matrigel, which was reported to be a highly efficient method of organoid formation for gynecological tumors. Recently, Lohmussaar et al. (2021) and Seol et al. (2022) reported organoid formation by using the Matrigel dome method, in which organoids were embedded inside Matrigel drops [13,14]. All these groups have utilized different protocols and different media compositions for cervical cancer organoid establishment. In the present study, cervical cancer organoids have been established using a modified protocol and have been extensively characterized. Moreover, it is important to cryopreserve the organoids without loss of parental characteristics for use in research and medical purposes as and when required. Although various protocols have been established to generate organoids from different tissues [15–17], studies investigating the retention of original tumoral characteristics in Cervical Cancer OrganoidS (CERCOS) post-cryopreservation remain limited. Therefore, we have also shown that organoids retain the morphological and histopathological features of the parental tumor tissue post-cryopreservation.

2. Materials and Methods

2.1. Patient Sample Collection

Biopsy samples were collected from treatment-naïve patients diagnosed with cervical cancer (squamous cell carcinoma/adenocarcinoma) as per the approval of the Institute Ethics Committee (IEC no. PGI/IEC/2020/000365). The collection of each sample was supervised by the consulting gynecologist and pathologist.

2.2. Tissue Processing

Patient tissue samples were collected in ice-cold PBS and brought to the laboratory within 10 min. The sample was washed thoroughly with ice-cold PBS thrice and dissected into small pieces (2–3 mm each) using forceps and a blade. The dissected tissue pieces were then treated with Collagenase I (1 mg/mL) for approximately 1–1.5 h and passed through a 70 µm cell strainer to obtain a single-cell suspension. The cells were then treated with 5 mL ACK lysis buffer (Gibco™, Thermo Fisher Scientific, Grand Island, NY, USA) for 5 min for

RBC lysis. The obtained cell pellet was resuspended in organoid medium (Table S1) and seeded on Matrigel Growth Factor Reduced (Matrigel GFR, Corning, Bedford, MA, USA) according to different culture methods followed.

2.3. Matrigel Dome Method

In the Matrigel dome method [1], the single-cell suspension was resuspended in GFR Matrigel and seeded as drops of 10 µL on a pre-warmed 24-well culture plate. The drops were allowed to solidify for 20 min at 37 °C, followed by addition of organoid media.

2.4. Matrigel Bilayer Organoid Culture (MBOC) Method

The MBOC protocol was followed as described by Maru et al. [18]. Matrigel GFR was pre-solidified on a 24-well culture plate and then seeded with a single-cell suspension. It was incubated overnight to allow the cells to attach. The next day, the floating cells were removed, and attached cells were overlaid with another layer of Matrigel. It was allowed to solidify and then overlaid with media.

2.5. Matrigel Single-Layer Method

In this method, a 24-well culture plate was coated with Matrigel GFR. Following the solidification of the Matrigel, the single-cell suspension was seeded onto coated wells and allowed to attach and proliferate.

2.6. Immunofluorescence Staining

The organoids were washed with ice-cold PBS and fixed in 4% PFA for 45 min, followed by treatment with 0.1% Triton-X for 15 min and blocking reagent (1% BSA) for 45 min. The organoids were then incubated with phalloidin dye for 1 h, followed by DAPI for 20 min. Then the organoids were mounted with an anti-fade mountant and visualized using an Olympus FV3000 confocal microscope (Olympus Corporation, Tokyo, Japan).

2.7. Scanning Electron Microscopy

Organoids were fixed in 2.5% glutaraldehyde overnight at 4 °C, followed by a PBS wash. The fixed organoids were then dehydrated by washing with a series of ethanol gradients (35% to 100%). Then, the organoids were air-dried and mounted on a stub using double-stick carbon tape. The organoids were sputter-coated with gold, and then images were acquired on a JEOL—JSM-IT300 InTouchScope™ Scanning Electron Microscope (JEOL Ltd., Akishima, Tokyo, Japan).

2.8. Histology and Immunohistochemistry

Histology and immunohistochemistry studies were performed on 10-day-old organoids. The organoids were fixed in 4% PFA overnight at 4 °C. Then, the organoids were embedded in paraffin blocks, and sections were cut and hydrated before staining. The sections were then processed for H&E staining and immunohistochemistry by incubation with antibodies against specific marker proteinsImages were captured using an Olympus BX53F2 brightfield microscope (Olympus Corporation, Tokyo, Japan).

2.9. Whole-Exome Sequencing

For whole-exome sequencing, DNA from tissue as well as collected organoids was isolated using DNeasy Tissue and Blood Kit, respectively (Qiagen GmbH, Hilden, Germany), following the manufacturer's instructions. The isolated DNA was checked for quality on a Qubit 4.0 fluorometer (Invitrogen™, Thermo Fisher Scientific, Waltham, MA, USA) before proceeding for library preparation. Library preparation involved enzymatic fragmentation followed by barcode adapter ligation, amplification, magnetic bead-based

purification and then target enrichment using an exome panel (Twist exome v2.0) and hybridization and amplification mix. Final libraries were quantified by qubit fluorometer and then normalized and loaded on NovaSeq-6000 Flow-cell (llumina Inc., San Diego, CA, USA) for PEx150bp and 100× mean depth sequencing. Raw data was demultiplexed and quality-checked using FastQC, followed by alignment to a reference genome (hg38). The bam files were subjected to duplicate removal using Picard tools, and variant calling was performed using Mutect-2 (GATK v4.4.0.0) and CNVkit (v0.9.9). Variant annotation was performed with Annovar, followed by variant analysis. The counts for variants and genes common between organoids and tissue and specific to only tissue and organoids, respectively, were listed using Mutect-2. Further, the common genes between organoids and tissue samples were mapped to the cervical cancer genes from cBio Portal to shortlist the important genes related to cervical cancer development. The software, along with the versions used for different purposes, is listed in Table S2.

2.10. Variant Filtering and Annotation

Raw variants identified by WES were subjected to sequential filtering to retain high-confidence variants. Variants with a population allele frequency $\geq$0.001 in the ExAC database, sequencing coverage (<5 reads) and minimum variant-supporting reads (<2) were removed. Variants predicted to be benign by SIFT and MutationTaster were also excluded. The remaining variants were categorized as per ACMG and AMP criteria. The filtered variants were then mapped with the cervical cancer-related genes taken from cBioportal and the COSMIC database. As matched normal DNA was unavailable, the somatic origin of these variants could not be definitively established.

2.11. CNV Analysis

CNV analysis was performed using a CNVkit based on normalized read-depth information obtained from WES data. Copy-number alterations were inferred from normalized sequencing coverage, followed by segmentation of genomic regions with similar copy-number profiles. The resulting CNV profiles were used to compare the genomic alterations observed in PDOs with those in their corresponding parental tumor tissues. The relative change in CNV signal between matched PDO and parental tumor samples was expressed as log fold change (logFC), calculated as the log2 ratio of the CNV signal in the PDO relative to that in the corresponding parental tumor tissues. Positive logFC values indicated a relative increase, whereas negative values indicated a relative decrease in the inferred CNV signal in PDOs compared with the corresponding parental tumor tissues. These values represent relative differences in inferred copy-number signal and were not interpreted as absolute copy-number values.

2.12. HPV Genotyping

PCR was performed to determine the HPV status of the organoids and the tissue. Infection with any HPV subtype was determined using primers specific for the L1 region of the HPV genome. Further, PCR using type-specific primers for two major high-risk subtypes—HPV 16 and HPV 18—was also carried out. GAPDH was used as the housekeeping gene. The SiHa and HeLa cell lines were used as positive controls for HPV 16 and HPV 18, respectively. Details of the primers used can be found in Table S3.

2.13. Passaging of Organoids

To passage organoids, organoid media was removed from the wells and treated with Cell Recovery Solution (Corning, Bedford, MA, USA) at 4 °C for 1 h. After 1 h, the organoids were observed floating in the cell recovery solution. The floating organoids were collected, washed with ice-cold PBS, and centrifuged at 570 *g* for 5 min. The obtained organoid pellet

was then treated with 1× TrypLE Express enzyme for 5 min to dissociate the organoids into small clusters of cells. The resulting cell pellet was seeded at a 1:3 ratio in 24-well plates pre-coated with GFR Matrigel.

2.14. Cryopreservation and Revival of Organoids

The collected organoids were dissociated using TrypLE, followed by resuspending the pellet in the Bambanker® freezing medium (GC Lymphotec Inc., Tokyo, Japan) and storing at −80 °C. The organoids were not dissociated to single cells. The cryogenic vial with the cryopreserved organoids was incubated for 1–3 min at 37 °C. Thereafter, AdDMEM/F12 +++ was added dropwise into the cryogenic vial. The organoids were centrifuged at 370 *g* for 5 min, and the pellet was resuspended in organoid medium, seeded on Matrigel and incubated at 37 °C and 5% CO_2.

2.15. Statistical Analysis

GraphPad Prism 8.0.2 software was used for statistical analysis. Data are presented as mean ± SEM. Data were analyzed by two-way ANOVA for three or more groups. p-value < 0.05 was considered statistically significant.

3. Results

3.1. Optimization of Organoid Culture

Figure 1 illustrates the utilization of various approaches to optimize organoid culture. The three methods were initially evaluated using different tumor samples to optimize and standardize the organoid culture conditions. To minimize the potential influence of inter-patient variability on comparative assessment, a subsequent head-to-head comparison of all three methods was performed using tissue obtained from the same patient. The results from this within-patient comparison were used to assess the relative efficiency of the three culture approaches. We did not observe satisfactory organoid formation with the Matrigel drop method in any of the patient samples (n = 5) (Figure 1). In the case of the MBOC protocol (n = 3), organoids began to form in two of the three samples within a span of just four days; however, they exhibited reduced structural integrity during culture, with small, irregular and loosely organized cellular aggregates and dispersed cells, rather than well-defined compact three-dimensional structures. We then modified the MBOC protocol by using only the lower layer of Matrigel, calling it 'Matrigel single-layer method'. The organoids generated using the modified protocol maintained a compact and well-defined three-dimensional architecture with improved structural stability during culture. This method yielded larger organoids (n = 5) within a timeframe of 4 to 7 days, with the potential for proliferation observed up to day 13 (Figure 1b).

3.2. Establishment of Patient-Derived Organoids (PDOs) Using Matrigel Single-Layer Method

PDOs were successfully generated from biopsy samples obtained from five patients and were designated as PDO1 to PDO5. The clinical data of the patients is given in Table 1. PDO1, PDO3, PDO4 and PDO5 were established from patients diagnosed with cervical squamous cell carcinoma, whereas PDO2 was established from a patient diagnosed with cervical adenocarcinoma. The age of the patients ranged from 42 to 60 years. Representative bright-field images of the established PDO lines are shown in Figure 2a. Since individual PDO cultures exhibited variable growth rates, images were selected at stages when well-defined organoid structures were observed. We observed variability in morphology among different PDOs, ranging from compact, round morphology to grape-like morphology (Figure 2a). The average size of 7-day-old PDOs was 177 µm (n = 5). There was also variation in the proliferation potential of the PDOs, as depicted in Figure 2d. Some PDOs

proliferated well and thus were characterized thoroughly, and they were cryopreserved as well. The characteristics of the patient samples and the derived organoids are given in Table 2.

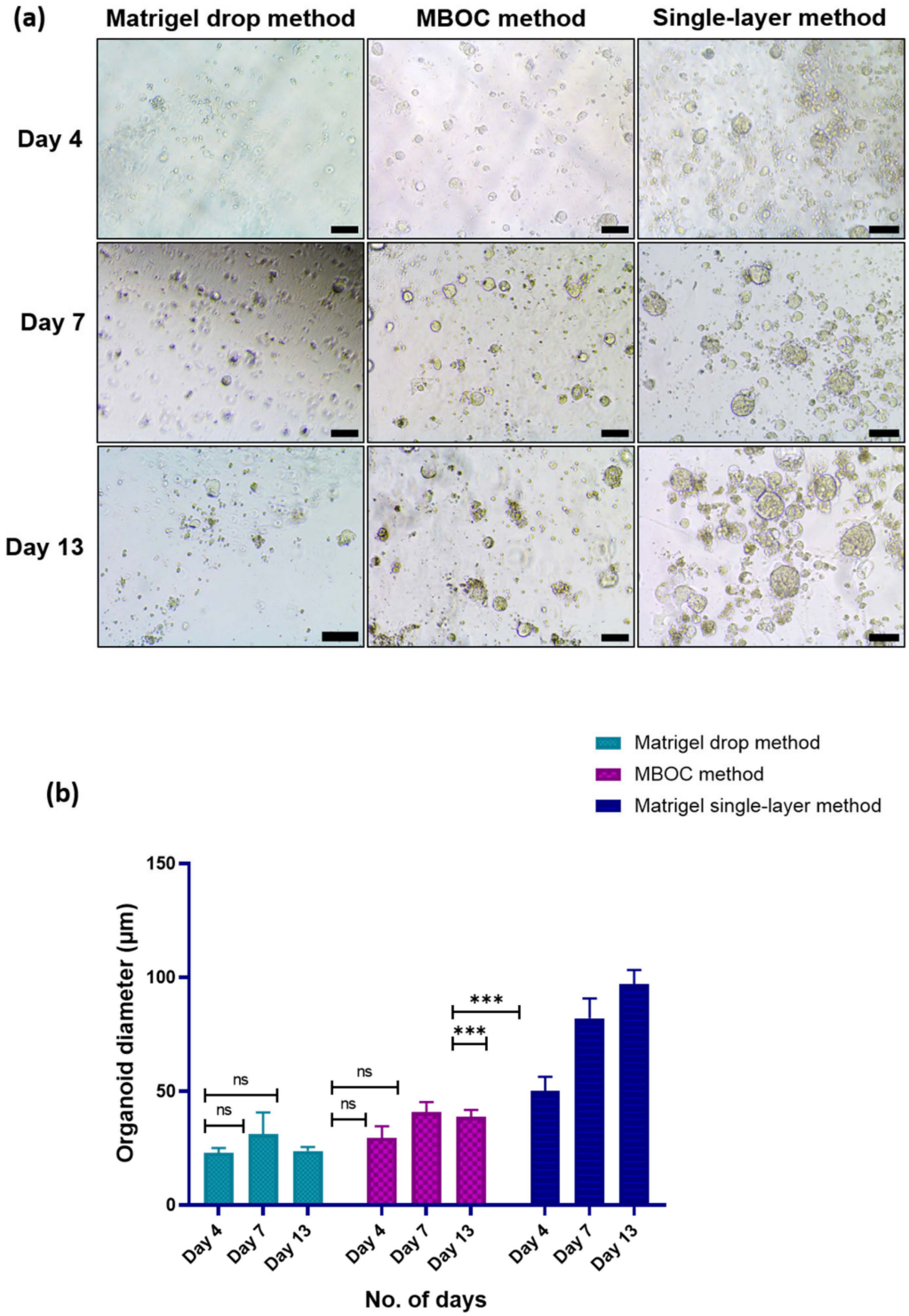

Figure 1. Comparison of different methods for organoid generation. (**a**) Representative images comparing three different methods (Matrigel dome method, Matrigel Bilayer Organoid Culture method (MBOC) and Matrigel single-layer method) employed for organoid generation. Images were taken at different days (day 4, day 7 and day 13); (scale bar, 500 µm). (**b**) Graphical comparison of organoid diameter measured by the three methods at different time points. Data are presented as Mean ± SEM (ns = $p > 0.05$, *** = $p \leq 0.001$).

Table 1. Clinical data of the patients included in this study.

Patient ID	Age	Cervical Cancer Subtype	Sampling Event	Tumor Grade (Code)	Tumor FIGO Stage	Treatment Status
P1	43	Squamous cell carcinoma, NOS	Biopsy	-	IIB	Treatment naïve
P2	50	Adenocarcinoma in situ	Biopsy	-	IIB	Treatment naïve
P3	60	Moderately differentiated squamous cell carcinoma	Biopsy	2	IIB	Treatment naïve
P4	49	Moderately differentiated squamous cell carcinoma	Biopsy	2	IIIC	Treatment naïve
P5	42	Moderately differentiated squamous cell carcinoma	Biopsy	2	IIIC	Treatment naïve

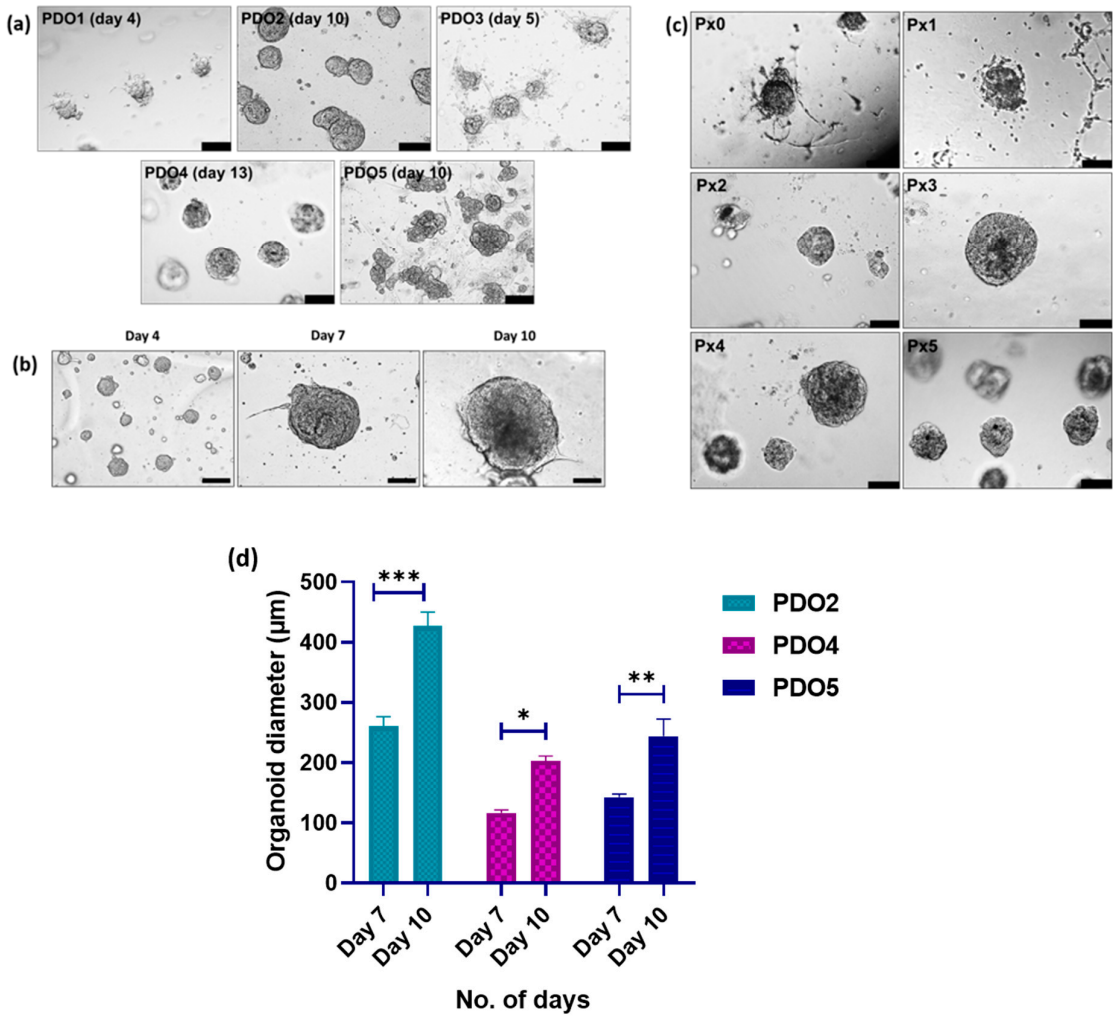

Figure 2. Establishment and expansion of organoids. (**a**) Bright-field microscopy showing different morphologies of cervical cancer organoids, from solid to grape-like morphology. Images are shown at the culture time points when well-defined organoid structures were observed, as the PDO lines exhibited variable growth and developmental kinetics. (**b**) Representative bright-field images showing organoid growth (PDO2) at different time points. (**c**) Bright-field images of organoids (PDO4) at different passages showing the expansion and proliferation of organoids (Px0 to Px5). (Scale bar, 500 µm). (**d**) Quantitative representation of organoid growth at different time points showing variable proliferation potential of PDOs. The experiment was performed in three independent biological replicates, and data are represented as Mean ± SEM (* = $p \leq 0.05$, ** = $p \leq 0.01$, *** = $p \leq 0.001$).

Table 2. Characteristics of patient samples and the derived organoids.

Patient Id	PDO Id	Age	Cervical Cancer Subtype	Expansion	HPV Typing	Histological Characterization	Whole-Exome Sequencing	Cryopreservation
P1	PDO1	43	Squamous Cell Carcinoma	–	–	+	–	–
P2	PDO2	50	Adenocarcinoma	+	+	+	+	–
P3	PDO3	60	Squamous Cell Carcinoma	–	–	–	–	–
P4	PDO4	49	Squamous Cell Carcinoma	+	+	+	+	+
P5	PDO5	42	Squamous Cell Carcinoma	+	+	+	+	+

+ Performed; – Not performed.

3.3. Expansion of PDOs

Organoids were passaged after reaching a size of approximately 150 µm. It was observed that the ability of organoid expansion varied from sample to sample. We could successfully passage two PDOs (PDO4 and PDO5) for more than two months (Figure 2b). The passaged organoids attained a larger size much earlier than the parental organoids, approximately 230 µm within 7–10 days.

3.4. Visualization of Actin Cytoskeleton

Actin filaments are involved in cell adhesion, cell shape and cell migration, and their arrangement facilitates 3D structure formation. To visualize the arrangement of actin filaments in organoids, phalloidin staining was performed. Phalloidin staining showed a peripheral arrangement of actin filaments (red) with the nucleus in the center (blue) (Figure 3a). This observed organization of actin filaments was consistent with the development of well-organized 3D organoid structures.

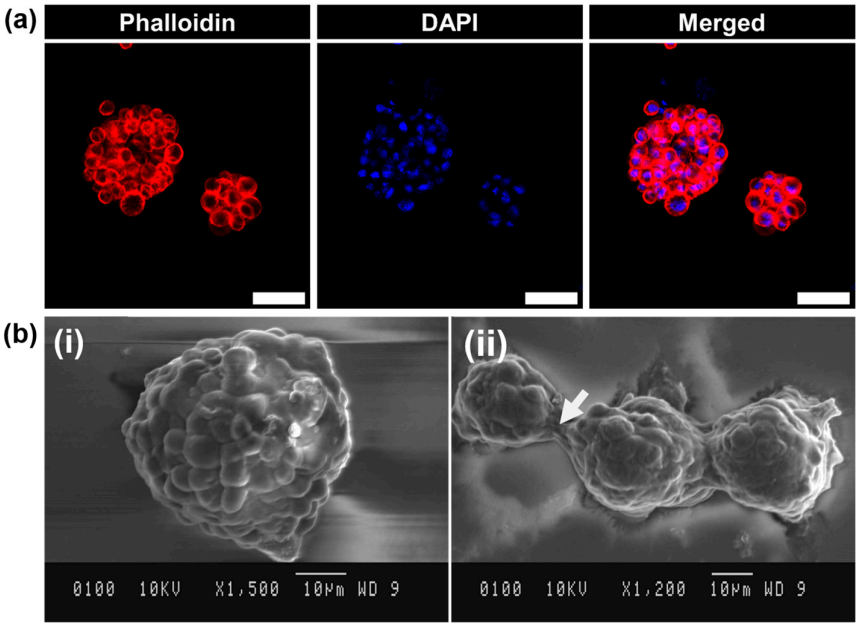

Figure 3. Structural analysis of organoids through phalloidin staining and scanning electron microscopy (SEM). (**a**) Visualization of arrangement of actin filaments using Phalloidin staining (Red—Phalloidin, Blue—DAPI) (scale bar, 50 µm). (**b**) (**i**) Analysis of ultrastructure of revived PDO4 using scanning electron microscopy (SEM) (×1500). (**ii**) White arrow showing cell–cell connections between PDOs (×1200).

3.5. Analysis of Ultrastructure by SEM

SEM imaging of PDOs for ultrastructural analysis showed strong cell–cell interactions forming a compact and smooth profile as illustrated in Figure 3b. Bulging cells were observed in some organoids, along with several short processes resembling microvilli and blebs, which contributed to an irregular surface. A connecting bridge (white arrow in Figure 3b(ii)) was observed between adjacent spheroids, indicating cellular protrusions or fusion between the organoids [19,20].

3.6. Histology and Immunohistochemical Analysis

To assess the histological similarity between the established PDOs and the corresponding patient tissues, both the PDOs and the corresponding tissues were subjected to histological and immunohistochemical analysis (passage 2–4). It was observed that PDOs retained the histological features of the tissue of origin. PDO2 showed glandular arrangement of cells corresponding to the adenocarcinoma subtype of the parental tumor tissue. PDO4 and PDO5 showed histological features similar to those of the parental squamous cell carcinoma tissues. IHC staining demonstrated preservation of characteristic marker expression patterns in the PDOs as observed in the corresponding parental tumors (Figure 4). PDO2 showed positive expression of P16 and CK7. PDO4 and PDO5 showed positive expression of P16, CK7 and P40.

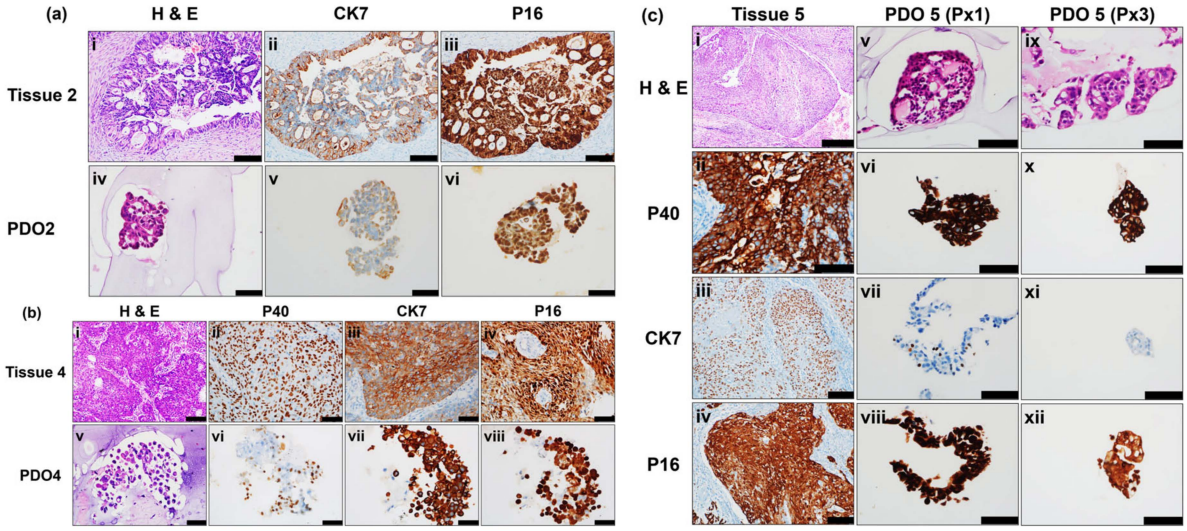

Figure 4. Comparative histological and immunohistochemical characterization of parental cervical tumor tissues and corresponding PDOs. (**a**) Representative images of the parental tumor tissue and corresponding PDOs from Patient sample 2. Panels (**i–iii**) show H&E, CK7 and P16 in the parental tissue, while panels (**iv–vi**) show the corresponding staining in PDOs. (**b**) Representative images from Patient sample 4, with panels (**i–iv**) representing parental tumor tissue and panels (**v–viii**) representing the corresponding PDOs. (**c**) Representative images from Patient sample 5, with panels (**i–iv**) representing parental tumor tissue and panels (**v–viii**) representing the corresponding PDOs at Passage 1 and panels (**ix–xii**) representing the corresponding PDOs at Passage 3. (Scale bars: 200 µm in (**a**(**i–iii**),**b**(**i**),**c**(**iii**,**iv**)); 100 µm in (**a**(**iv–vi**),**b**(**ii–viii**),**c**(**ii**,**v–xii**)); 500 µm in (**c**(**i**))).

3.7. Retention of HPV Genotype in Patient-Derived Organoids

HPV typing was performed for three pairs of PDOs and their corresponding parental tumor tissues that showed similarity between HPV status of the parental tumor tissue and the derived PDOs (Figure S1). All of the patients were HPV-positive; however, HPV16 was lost in PDO2.

3.8. Whole-Exome Sequencing Data from Tissues and Corresponding Organoids

Whole-exome sequencing of three tissue samples (Tissue 2, Tissue 4 and Tissue 5) and their corresponding PDOs (PDO2, PDO4 and PDO5) was performed at a mean depth of 100×, and variant calling was performed using Mutect2. Mutect2 identified a total of 340,404, 391,516 and 423,218 variants in Tissue 2, Tissue 4 and Tissue 5, respectively. A total of 549,290, 429,588 and 389,839 variants were identified in PDO2, PDO4 and PDO5, respectively. An average of 385,016 variants were identified across the three tissue samples, compared with 456,239 variants across the three PDOs. Out of these, 95,224, 83,947 and 97,067 variants were common between tissue 2 and PDO2, tissue 4 and PDO4, and tissue 5 and PDO5, respectively (Figure S2).

3.9. Common Variants Related to Cervical Cancer Development

The identified common variants between the patient tissues and corresponding PDOs were then uploaded to cBioPortal. All the variants and associated genes reported in cervical cancer-related studies and present in cBioPortal, even at a very low allele frequency, were taken). Following the variant filtering, cervical cancer tissues were found to harbor a higher number of variants compared to their paired organoids, likely due to the selective growth of less aberrant cell subpopulations in culture (Figure S3). The filtered variants were then mapped to cervical cancer-related genes taken from cBioPortal and the COSMIC database. The results showed that PDO2 and PDO5 showed 50% concordance with the paired tissue, whereas PDO4 shared 31% concordance with the paired tissue (Figure 5a). Among the top common mutated genes were *LRP1B*, *KMT2A*, *MET*, *TTN*, *PIK3CA* and *NF1*. Mutations in some cancer-related genes, such as *MTOR*, *ALK*, *KMT2C* and *KMT2D,* were found to be lost in the derived organoids. The genes that were found to be mutated in more than one sample were SMO, TTN and VEGFA. We further analyzed base variants in cervical cancer tumor and organoids. The distribution of point mutation types in the parental tumor tissue was largely conserved in the derived organoids, with C > T being the dominant base variant type (Figure 5b). We have also plotted single-nucleotide polymorphism (SNP) density plots of tissues and PDOs after applying filtering criteria. It was observed that SNP density was reduced in the PDOs compared with the corresponding tissues (Figure 5c).

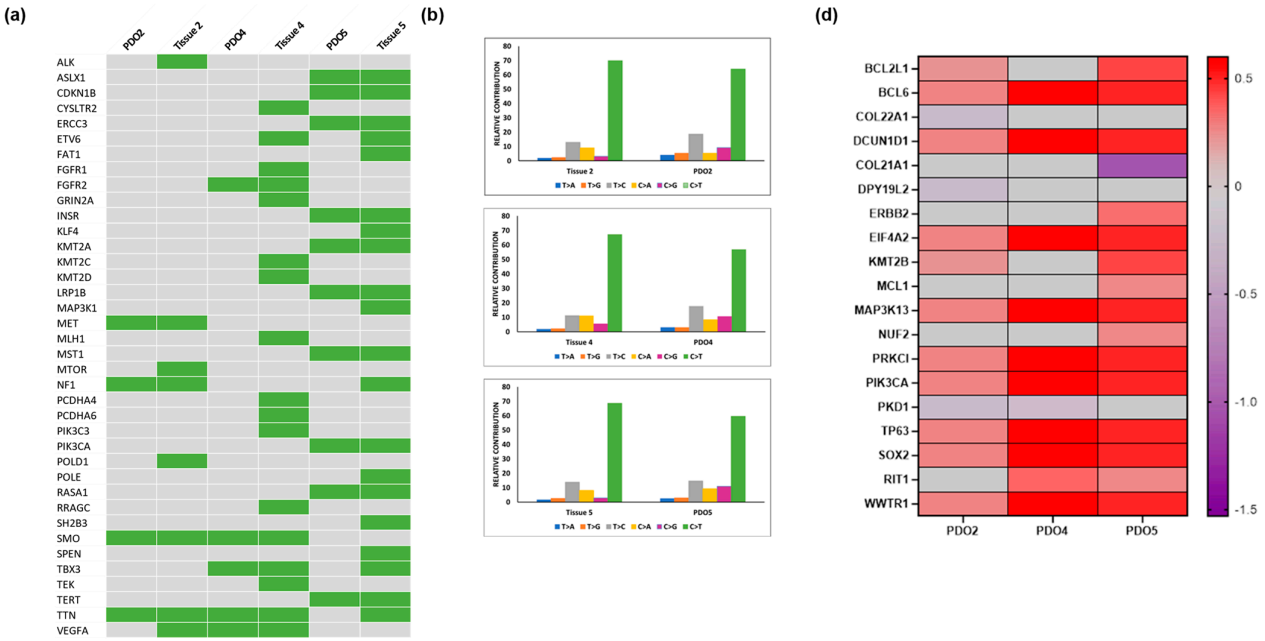

Figure 5. *Cont.*

(c)

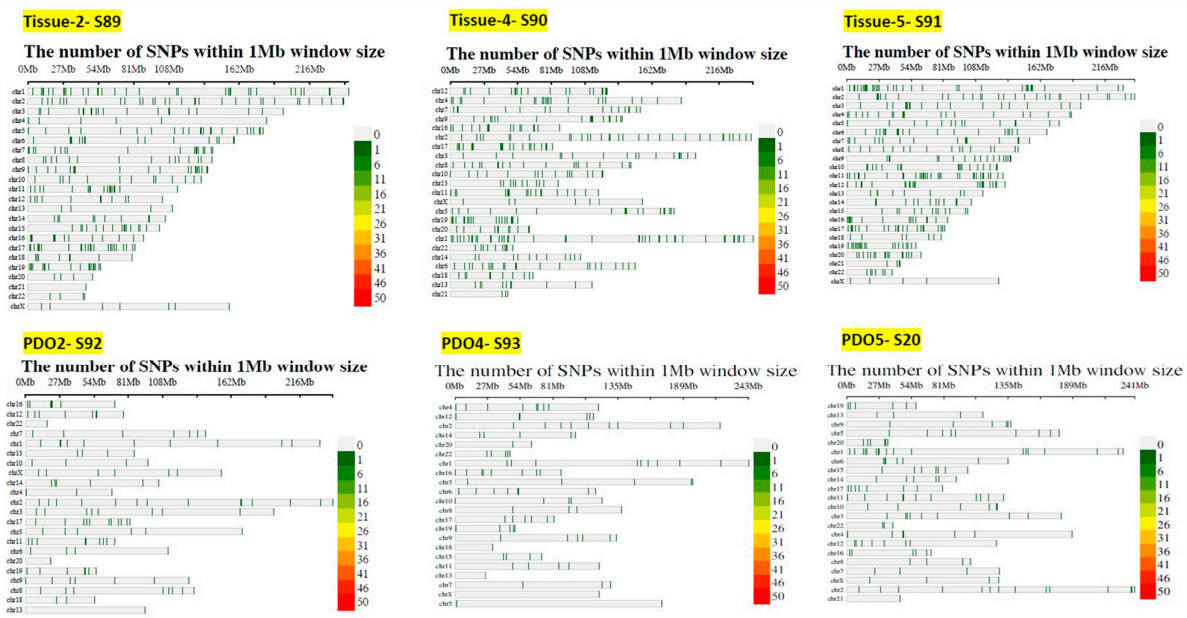

Figure 5. Comparison of mutational landscape of organoids and the corresponding parental tumor tissues through WES. (**a**) Mutation matrix comparing the cancer-associated mutated variants in cervical cancer organoids with those in parental tumor tissues (Green–variant observed). (**b**) Bar plots showing the frequencies of the six types of point mutations in the parental tumor tissues and the derived organoids, with C > T being the dominant SNV type. (**c**) SNP density plots showing reduction in SNP density in PDOs compared to corresponding tissues. (**d**) Heat map showing log fold change (logFC) of CNV signal in PDOs relative to their corresponding parental tumor tissues. Positive and negative logFC values indicate relative increases and decreases, respectively, in the inferred copy-number signal in PDOs compared with parental tumors.

3.10. Copy Number Variation (CNV) Calling

The CNVkit tool was used for CNV calling in the tissues and the PDOs. The tissue samples were taken as the reference to calculate the log fold change in CNVs in the corresponding PDOs (Table S4). The top 20 genes showing CNV gains in cervical cancer according to the COSMIC database exhibited a relative increase in CNV signal in the three PDOs, and all the genes were found to be localized on chr 3. When copy number alterations present in cBioPortal with a frequency >10% were compared, 25 genes exhibited a fold change in CNV in PDO2, 31 genes in PDO4 and 36 genes in PDO5. Among them, *ATR* (3q23), *SOX2* (3q26.33), *BCL6* (3q27.3), *EIF4A2* (3q27.3), *PRKCI* (3q26.2), *PIK3CA* (3q26.32), *TP63* (3q28), *DCUN1D1* (3q26.33), *FGF12* (3q28-q29) and *MAP3K13* (3q27.2) were the most commonly amplified genes (Figure 5d).

3.11. Characterization of PDOs After Cryopreservation and Revival

PDOs were cryopreserved and revived after one month. Initially, there was slow proliferation of the revived organoids. The PDOs took approximately 11 days to resume proliferation, after which they were passaged. Following the passage, there was an increase in proliferation rate, with organoids forming within 7 days (Figure 6a).

3.12. Histology

Histological analysis showed preservation of the characteristic features of squamous cell carcinoma. Further, IHC analysis of the revived organoids showed expression of diagnostic markers p63 and CK7 comparable to that observed in the original tissue, indicating preservation of the histological subtype after cryopreservation (Figure 6b).

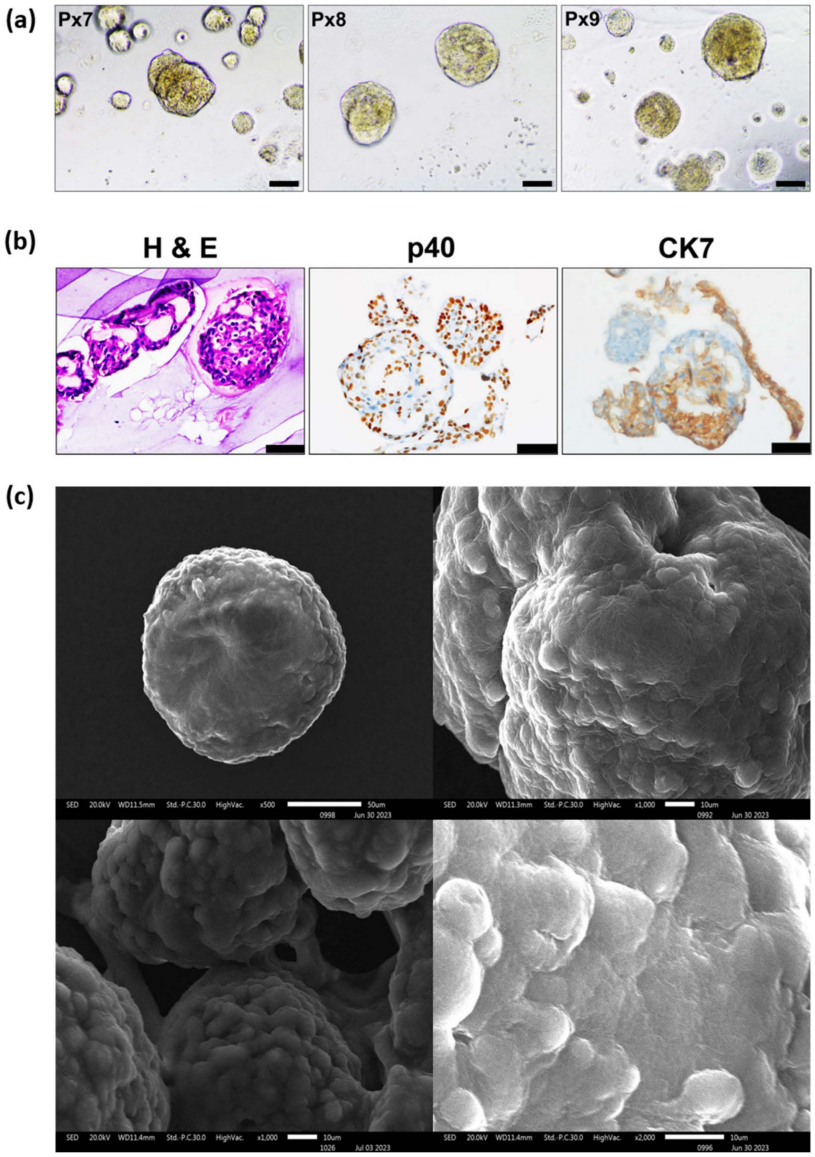

Figure 6. Characterization of PDOs post-cryopreservation and revival. (**a**) Bright-field images of PDO4 at different passages (Px6, Px7 and Px8) post-cryopreservation and revival (Scale bar, 500 µm). (**b**) Histological and IHC analysis of revived PDOs showing morphology and expression of cell surface markers (p40 and CK7) post-cryopreservation (Scale bar, 100 µm). (**c**) Analysis of ultrastructure of revived PDO4 using scanning electron microscopy (SEM) (×500, ×1000 and ×2000).

3.13. SEM

Morphological analysis of the revived organoids using SEM showed compact and round morphology, indicating preservation of cell–cell connections (Figure 6c).

4. Discussion

PDO models have been reported to successfully recapitulate the intra- and inter-tumor heterogeneity. These models serve as a bridge between conventional in vitro models and in vivo models and have immense potential for clinical applications, particularly in the field of cancer. PDO models more closely mimic the tumor tissue phenotype compared to conventional 2D cultures. Studies have demonstrated concordance in drug responses between organoids and corresponding patients, making them a suitable platform to predict therapeutic responses in several cancers [15,17,21–23].

In the present study, we optimized the organoid culture conditions and observed that a simple modification of the Matrigel single-layer method was effective for establishing organoids from different subtypes of cervical cancer. The Matrigel dome method has been widely adopted for organoid generation in various cancers, including breast, lung, pancreatic, ovarian and rectal cancer [5,13–15,18]. However, in the present study, the Matrigel dome method did not produce satisfactory organoids from cervical cancer tissues even after 14–20 days, which is within the usual period reported for organoid generation using this method. This is probably due to the accumulation of detrimental factors released from dead cells trapped within the dome, as reported previously [12]. The Modified Matrigel Bilayer Organoid Culture (MBOC) protocol has been reported to capture highly proliferative stem cell-like cell populations without conducting cell-sorting in gynecological tumors [18]; therefore, this method was evaluated for organoid formation. Although organoids were formed within 4–7 days using the MBOC protocol, they subsequently disintegrated. We hypothesized that the presence of the upper layer of Matrigel might limit effective organoid proliferation. Consequently, only the lower layer of Matrigel was utilized, and this modification in the protocol was termed the 'Matrigel Single-Layer Method'. This method generated comparatively larger organoids (~150 µm) within a shorter period (generally 7–10 days) that were passaged successfully. Therefore, this modified method of cervical organoid generation was adopted for further characterization.

Our results showed that the PDOs could be successfully recovered from the Matrigel after culture using the Matrigel Single-Layer Method. In our study, Matrigel was depolymerized using Cell Recovery solution, and the organoids were collected without vigorous pipetting or scraping, which often compromises the viability of PDOs. This method offers an advantage over the Matrigel dome method, in which scraping and pipetting may sometimes be required to release the organoids from the dome [24,25]. However, the organoids showed variability in their ability to undergo long-term expansion, which may be attributed to intratumoral heterogeneity, proliferative capacity and genetic and epigenetic characteristics. In addition, technical factors such as tissue quality, the initial number of tumor cells and adaptation to 3D culture conditions may influence organoid establishment and long-term expansion. Further optimization of culture conditions will be important to enhance reproducibility of cervical cancer organoid cultures.

Actin filaments play an important role in maintaining the cytoskeleton of 3D structures. Polymerization of actin filaments promotes initial cell–cell contact and cell compaction through cytoskeletal remodeling. Studies have reported that disruption of F-actin by cytochalasin D leads to the formation of loose structures rather than tight spheroids [26–28]. The observed F-actin arrangement within the PDOs therefore provides morphological evidence of cytoskeletal organization involved in development of three-dimensional cellular structures. These findings are consistent with the concept proposed by Lancaster and Knoblich, wherein coordinated cell–cell and cell–matrix interactions are involved in self-cellular organization of the organoids [29].

Histological examination by H&E demonstrated organized epithelial structures with morphological features consistent with the parental tumor. Immunohistochemical characterization further confirmed their epithelial and cervical tumor phenotype, with positive expression of epithelial/cervical cancer-associated markers, including CK7, p40 and p16. Further, the comparable expression of IHC markers in the PDOs and the corresponding parental tumors showed preservation of histological characteristics in the established PDOs. Although HPV analysis was performed only in a subset of samples with a sufficient amount of DNA, the PDOs retained HPV status similar to that of their corresponding parental tumors. This supports their potential as models to understand the pathophysiology of HPV-associated cervical cancer. Notably, HPV16 was not detected in PDO2, suggesting

a possible shift from an HPV-dependent to an HPV-independent state, in which tumor cells may no longer rely on viral oncoproteins for growth and proliferation. The loss of HPV16 may also reflect that viral characteristics may change during in vitro culture. Consistent with this, Park et al. reported the loss of the HPV 16 E7 oncogene in cervical lesions arising in Fanconi anemia pathway-deficient mice due to accumulation of mutations in cellular genes [30]. Such loss indicates the development of resistance to HPV-targeting therapies and underscores the importance of HPV genotyping to track viral persistence in organoid-based drug screening.

The ability to cryopreserve and recover PDOs provides an important clinical advantage for their long-term use. The cryopreservation was done using a simple method involving resuspension of the cell pellet in the freezing medium [16]. However, detailed post-thaw characterization was performed only on PDO4; therefore, the preservation of organoid characteristics cannot be generalized to all established PDOs. Further validation across multiple PDOs is required to establish the reproducibility of the findings.

One of the important features of organoids is that they maintain the mutational landscape of the parental tumor. PDOs demonstrated partial genomic concordance, with 31–50% of the identified variants shared with the corresponding parental tumor, indicating preservation of a subset of the parental tumor-associated variants. The absence of some cancer-associated variants in PDOs may reflect culture-driven clonal selection, whereby specific tumor cell populations are preferentially enriched during culture. Additionally, intratumoral heterogeneity and differences in the cellular composition of the tissue used for organoid establishment may contribute to the observed genomic differences. Since matched normal DNA could not be obtained from the cervical cancer patients included in this study, WES analysis could not definitively distinguish between somatic and germline variants. Although population frequency databases were used during variant filtering to exclude common germline variants, the possibility of rare germline variants could not be ruled out.

The most frequent mutation identified was in the titin (TTN) gene, which was present in all three patient tissues and two organoids (PDO2 and PDO4) but absent in PDO5. TTN plays a crucial role in cardiac and skeletal muscles and has been associated with increased mutation load, improved responses to immune checkpoint therapy, and longer survival in various solid tumors, including cervical cancer [31]. Another commonly mutated cervical cancer gene in squamous cell carcinoma (28%) is PIK3CA, with the E545K mutation being a major hotspot mutation [32]. This mutation causes abnormal cell proliferation and reduced apoptosis, which have been linked to cervical cancer development. Another mutated gene was Smoothened (SMO), a conserved signal transducer of the Sonic Hedgehog pathway. Various studies have reported the role of the Hedgehog signaling pathway in mediating chemo-radiotherapy resistance and regulating stem cell characteristics during EMT in cervical cancer [33–36]. An increase in CNV signal in PDOs compared with the original tumor may be attributed to the high proliferative potential of stem cells forming the organoids and the effects of in vitro culture conditions, including the addition of external growth factors [37–39].

A major limitation of the present study is the relatively small number of patient-derived cervical cancer organoids (n = 5), which limits the statistical power and generalizability of the findings. Although the established organoids retained key morphological and molecular characteristics of cervical cancer, a larger and more clinically diverse cohort is required to capture the inter-patient heterogeneity of cervical cancer and to validate the observations of the study. Future studies incorporating a larger number of PDOs, together with detailed clinical and genomic characterization, will be important to establish the translational relevance of this model.

5. Conclusions

The present study illustrates the successful establishment and characterization of PDOs using a modified and time-efficient culture system. The established PDOs demonstrated preservation of several characteristics of their corresponding parental tumors, including histological features, HPV status and a subset of genomic alterations. The histological features were also retained after cryopreservation. These findings highlight the potential of cervical cancer organoids as a platform for in vitro drug screening and patient-response prediction. However, prospective studies correlating the organoid drug responses with clinical outcomes are required to establish their predictive value and clinical utility in precision medicine.

Supplementary Materials: The following supporting information can be downloaded at: https://www.mdpi.com/article/10.3390/organoids5030031/s1, Table S1: Composition of the organoid medium used for establishing organoid culture. Table S2: Details of the software, along with the versions, that has been used for whole-exome sequencing. Table S3: Details of the primer used for HPV typing. Table S4: Log fold change values in CNVs in PDOs with reference to the parental tumor tissue. Figure S1: HPV typing of the organoids and tumor tissue showed the preservation of HPV status of the parental tumor tissues in PDO5 (A) and PDO4 (B). (NTC—Negative control, O—Organoid, T—Tissue, P—Positive Control (HeLa for HPV 18 and HPV 16 for SiHa). Figure S2: Venn diagram of the variants common in tissues and the corresponding PDOs. Figure S3: Number of variants after applying various filtering criteria to PDOs and tissues.

Author Contributions: Conceptualization: S.S. and S.B.; Data curation: S.S., R.B., R.S., P.B. and S.B.; Formal analysis: R.B., R.S., P.B. and S.B.; Funding acquisition: S.B.; Investigation: S.S., R.B., R.S. and S.B.; Methodology: S.S., P.B. and S.B.; Project administration: S.B.; Resources: S.B.; Software: P.B.; Supervision: R.B., R.S., P.B. and S.B.; Validation: S.S., R.B., R.S., P.B. and S.B.; Visualization: P.B. and S.B.; Roles/Writing—original draft: S.S.; and Writing—review and editing: R.B., R.S., P.B. and S.B. All authors have read and agreed to the published version of the manuscript.

Funding: This work was supported by the Indian Council of Medical Research (ICMR), India (Grant number—2020-4349).

Institutional Review Board Statement: Ethical approval was obtained from the Institutional Ethics Committee of PGIMER, Chandigarh for carrying out the study (IEC no. PGI/IEC/2020/000365, dated 4 May 2020). The samples were collected after obtaining written consent from all the patients.

Informed Consent Statement: Written consent was obtained from every patient.

Data Availability Statement: The original contributions presented in this study are included in the article/Supplementary Materials. Further inquiries can be directed to the corresponding authors.

Acknowledgments: S.S. acknowledges the Council of Scientific and Industrial Research (CSIR) for providing a research fellowship. The authors are grateful to the CSIC facility, PGIMER for carrying out Scanning Electron Microscopy.

Conflicts of Interest: The authors declare no conflicts of interest.

Abbreviations

CK7	Cytokeratin 7
CNV	Copy Number variation
GFR Matrigel	Growth Factor Reduced Matrigel
HPV	Human Papillomavirus
MBOC	Matrigel Bilayer organoid culture
PDO	Patient-derived organoids
SEM	Scanning Electron Microscope
SNP	Single-Nucleotide Polymorphism

References

1. Fang, Z.; Li, P.; Du, F.; Shang, L.; Li, L. The role of organoids in cancer research. *Exp. Hematol. Oncol.* **2023**, *12*, 69. [CrossRef]
2. Guillen, K.P.; Fujita, M.; Butterfield, A.J.; Scherer, S.D.; Bailey, M.H.; Chu, Z.; DeRose, Y.S.; Zhao, L.; Cortes-Sanchez, E.; Yang, C.-H.; et al. A human breast cancer-derived xenograft and organoid platform for drug discovery and precision oncology. *Nat. Cancer* **2022**, *3*, 232–250. [CrossRef]
3. Campaner, E.; Zannini, A.; Santorsola, M.; Bonazza, D.; Bottin, C.; Cancila, V.; Tripodo, C.; Bortul, M.; Zanconati, F.; Schoeftner, S.; et al. Breast cancer organoids model patient-specific response to drug treatment. *Cancers* **2020**, *12*, 3869. [CrossRef]
4. Tiriac, H.; Belleau, P.; Engle, D.D.; Plenker, D.; Deschenes, A.; Somerville, T.D.D.; Froeling, F.E.M.; Burkhart, R.A.; Denroche, R.E.; Jang, G.H.; et al. Organoid profiling identifies common responders to chemotherapy in pancreatic cancer. *Cancer Discov.* **2018**, *8*, 1112–1129. [CrossRef]
5. Kim, M.; Mun, H.; Sung, C.O.; Cho, E.J.; Jeon, H.-J.; Chun, S.-M.; Jung, D.J.; Shin, T.H.; Jeong, G.S.; Kim, D.K.; et al. Patient-derived lung cancer organoids as in vitro cancer models for therapeutic screening. *Nat. Commun.* **2019**, *10*, 3991. [CrossRef]
6. Ganesh, K.; Wu, C.; O'Rourke, K.P.; Szeglin, B.C.; Zheng, Y.; Sauvé, C.-E.G.; Adileh, M.; Wasserman, I.; Marco, M.R.; Kim, A.S.; et al. A rectal cancer organoid platform to study individual responses to chemoradiation. *Nat. Med.* **2019**, *25*, 1607–1614. [CrossRef]
7. Yao, Y.; Xu, X.; Yang, L.; Zhu, J.; Wan, J.; Shen, L.; Xia, F.; Fu, G.; Deng, Y.; Pan, M.; et al. Patient-Derived Organoids Predict Chemoradiation Responses of Locally Advanced Rectal Cancer. *Cell Stem Cell* **2020**, *26*, 17–26.e6. [CrossRef]
8. Kopper, O.; de Witte, C.J.; Lõhmussaar, K.; Valle-Inclan, J.E.; Hami, N.; Kester, L.; Balgobind, A.V.; Korving, J.; Proost, N.; Begthel, H.; et al. An organoid platform for ovarian cancer captures intra- and interpatient heterogeneity. *Nat. Med.* **2019**, *25*, 838–849. [CrossRef]
9. Nanki, Y.; Chiyoda, T.; Hirasawa, A.; Ookubo, A.; Itoh, M.; Ueno, M.; Akahane, T.; Kameyama, K.; Yamagami, W.; Kataoka, F.; et al. Patient-derived ovarian cancer organoids capture the genomic profiles of primary tumours applicable for drug sensitivity and resistance testing. *Sci. Rep.* **2020**, *10*, 12581. [CrossRef]
10. Sachs, N.; de Ligt, J.; Kopper, O.; Gogola, E.; Bounova, G.; Weeber, F.; Balgobind, A.V.; Wind, K.; Gracanin, A.; Begthel, H.; et al. A Living Biobank of Breast Cancer Organoids Captures Disease Heterogeneity. *Cell* **2018**, *172*, 373–386.e10. [CrossRef]
11. Villa, P.L.; Jackson, R.; Eade, S.; Escott, N.; Zehbe, I. Isolation of Biopsy-Derived, Human Cervical Keratinocytes Propagated as Monolayer and Organoid Cultures. *Sci. Rep.* **2018**, *8*, 17869. [CrossRef]
12. Maru, Y.; Tanaka, N.; Ebisawa, K.; Odaka, A.; Sugiyama, T.; Itami, M.; Hippo, Y. Establishment and characterization of patient-derived organoids from a young patient with cervical clear cell carcinoma. *Cancer Sci.* **2019**, *110*, 2992–3005. [CrossRef]
13. Seol, H.S.; Oh, J.H.; Choi, E.; Kim, S.; Kim, H.; Nam, E.J. Preclinical investigation of patient-derived cervical cancer organoids for precision medicine. *J. Gynecol. Oncol.* **2023**, *34*, e35. [CrossRef]
14. Lõhmussaar, K.; Oka, R.; Valle-Inclan, J.E.; Smits, M.H.; Wardak, H.; Korving, J.; Begthel, H.; Proost, N.; van de Ven, M.; Kranenburg, O.W.; et al. Patient-derived organoids model cervical tissue dynamics and viral oncogenesis in cervical cancer. *Cell Stem Cell* **2021**, *28*, 1380–1396.e6. [CrossRef]
15. Drost, J.; Clevers, H. Organoids in cancer research. *Nat. Rev. Cancer* **2018**, *18*, 407–418. [CrossRef]
16. Driehuis, E.; Kretzschmar, K.; Clevers, H. Establishment of patient-derived cancer organoids for drug-screening applications. *Nat. Protoc.* **2020**, *15*, 3380–3409, Correction in *Nat. Protoc.* **2021**, *16*, 5739. [CrossRef]
17. Ma, Y.S.; Yang, X.L.; Xin, R.; Wu, T.-M.; Shi, Y.; Zhang, D.D.; Wang, H.-M.; Wang, P.-Y.; Liu, J.-B.; Fu, D. The power and the promise of organoid models for cancer precision medicine with next-generation functional diagnostics and pharmaceutical exploitation. *Transl. Oncol.* **2021**, *14*, 101126. [CrossRef]
18. Maru, Y.; Tanaka, N.; Itami, M.; Hippo, Y. Efficient use of patient-derived organoids as a preclinical model for gynecologic tumors. *Gynecol. Oncol.* **2019**, *154*, 189–198. [CrossRef]
19. Deynoux, M.; Sunter, N.; Ducrocq, E.; Dakik, H.; Guibon, R.; Burlaud-Gaillard, J.; Brisson, L.; Rouleux-Bonnin, F.; Le Nail, L.-R.; Hérault, O.; et al. A comparative study of the capacity of mesenchymal stromal cell lines to form spheroids. *PLoS ONE* **2020**, *15*, e0225485. [CrossRef]
20. Ware, M.J.; Colbert, K.; Keshishian, V.; Ho, J.C.-S.; Corr, S.J.; Curley, S.A.; Godin, B. Generation of homogenous three-dimensional pancreatic cancer cell spheroids using an improved hanging drop technique. *Tissue Eng. Part C Methods* **2016**, *22*, 312–321. [CrossRef]
21. Clevers, H. Modeling Development and Disease with Organoids. *Cell* **2016**, *165*, 1586–1597. [CrossRef]
22. Zhou, Z.; Cong, L.; Cong, X. Patient-Derived Organoids in Precision Medicine: Drug Screening, Organoid-on-a-Chip and Living Organoid Biobank. *Front. Oncol.* **2021**, *11*, 762184. [CrossRef]
23. Kondo, J.; Inoue, M. Application of cancer organoid model for drug screening and personalized therapy. *Cells* **2019**, *8*, 470. [CrossRef]
24. Clinton, J.; McWilliams-Koeppen, P. Initiation, Expansion, and Cryopreservation of Human Primary Tissue-Derived Normal and Diseased Organoids in Embedded Three-Dimensional Culture. *Curr. Protoc. Cell Biol.* **2019**, *82*, e66. [CrossRef]

25. Ross, A.D.B.; Perrone, F.; Elmentaite, R.; Teichmann, S.A.; Zilbauer, M. Obtaining purified human intestinal epithelia for single-cell analysis and organoid culture. *STAR Protoc.* **2021**, *2*, 100597. [CrossRef]
26. Smyrek, I.; Mathew, B.; Fischer, S.C.; Lissek, S.M.; Becker, S.; Stelzer, E.H.K. E-cadherin, actin, microtubules and FAK dominate different spheroid formation phases and important elements of tissue integrity. *Biol. Open* **2019**, *8*, bio037051. [CrossRef]
27. Tzanakakis, E.S.; Hansen, L.K.; Hu, W.S. The Role of Actin Filaments and Microtubules in Hepatocyte Spheroid Self-Assembly. *Cell Motil. Cytoskelet.* **2001**, *48*, 175–189. [CrossRef]
28. Wulf, E.; Deboben, A.; Bautz, F.A.; Faulstich, H.; Wieland, T. Fluorescent phallotoxin, a tool for the visualization of cellular actin. *Proc. Natl. Acad. Sci. USA* **1979**, *76*, 4498–4502. [CrossRef]
29. Lancaster, M.A.; Knoblich, J.A. Organogenesis in a dish: Modeling development and disease using organoid technologies. *Science* **2014**, *345*, 1247125. [CrossRef]
30. Park, S.; Park, J.W.; Pitot, H.C.; Lambert, P.F. Loss of Dependence on Continued Expression of the Human Papillomavirus 16 E7 Oncogene in Cervical Cancers and Precancerous Lesions Arising in Fanconi Anemia Pathway-Deficient Mice. *mBio* **2016**, *7*, 3. [CrossRef]
31. Xu, Y.; Luo, H.; Hu, Q.; Zhu, H. Identification of Potential Driver Genes Based on Multi-Genomic Data in Cervical Cancer. *Front Genet.* **2021**, *12*, 598304. [CrossRef]
32. Zhang, Y. The effects of PIK3CA mutations on cervical cancer. *E3S Web Conf.* **2024**, *553*, 05025. [CrossRef]
33. Chaudary, N.; Pm, H.D.; Faw, M.M.; Hrp, C.B. Hedgehog pathway signaling in cervical carcinoma and outcome after chemoradiation. *Cancer* **2012**, *118*, 3105–3115. [CrossRef]
34. Sharma, A.; De, R.; Javed, S.; Srinivasan, R.; Pal, A.; Bhattacharyya, S. Sonic hedgehog pathway activation regulates cervical cancer stem cell characteristics during epithelial to mesenchymal transition. *J. Cell. Physiol.* **2019**, *234*, 15726–15741. [CrossRef]
35. Sharma, A.; Kaur, H.; De, R.; Srinivasan, R.; Pal, A.; Bhattacharyya, S. Knockdown of E-Cadherin induces cancer stem-cell-like phenotype and drug resistance in cervical cancer cells. *Biochem. Cell Biol.* **2021**, *99*, 587–595. [CrossRef]
36. Liu, C.; Wang, R. The Roles of Hedgehog Signaling Pathway in Radioresistance of Cervical Cancer. *Dose Response* **2019**, *17*, 1559325819885293. [CrossRef]
37. Boretto, M.; Maenhoudt, N.; Luo, X.; Hennes, A.; Boeckx, B.; Bui, B.; Heremans, R.; Perneel, L.; Kobayashi, H.; Van Zundert, I.; et al. Patient-derived organoids from endometrial disease capture clinical heterogeneity and are amenable to drug screening. *Nat. Cell Biol.* **2019**, *21*, 1041–1051. [CrossRef]
38. Chiaradia, I.; Imaz-Rosshandler, I.; Nilges, B.S.; Boulanger, J.; Pellegrini, L.; Das, R.; Kashikar, N.D.; Lancaster, M.A. Tissue morphology influences the temporal program of human brain organoid development. *Cell Stem Cell* **2023**, *30*, 1351–1367.e10. [CrossRef]
39. Li, Y.; Muffat, J.; Omer, A.; Bosch, I.; Lancaster, M.A.; Sur, M.; Gehrke, L.; Knoblich, J.A.; Jaenisch, R. Induction of Expansion and Folding in Human Cerebral Organoids. *Cell Stem Cell* **2017**, *20*, 385–396.e3. [CrossRef]